

Bistatic ISAC: Practical Challenges and Solutions

Lucas Giroto*, Marcus Henninger*, Alexander Felix*, Maximilian Bauhofer†, Taewon Jeong‡,
Umut Utku Erdem‡, Stephan ten Brink†, Thomas Zwick‡, Benjamin Nuss§, and Silvio Mandelli*

*Nokia Bell Labs Stuttgart, Germany

†Institute of Telecommunications, University of Stuttgart, Germany

‡Institute of Radio Frequency Engineering and Electronics, Karlsruhe Institute of Technology, Germany

§Professorship of Microwave Sensors and Sensor Systems, Technical University of Munich, Germany

E-mail: lucas.giroto@nokia-bell-labs.com

Abstract—This article presents and discusses challenges and solutions for practical issues in bistatic integrated sensing and communication (ISAC) in 6G networks. Considering orthogonal frequency-division multiplexing as the adopted waveform, a discussion on system design aiming to achieve both a desired sensing key performance indicators and limit the impact of hardware impairments is presented. In addition, signal processing techniques to enable over-the-air synchronization and generation of periodograms with range, Doppler shift, and angular information are discussed. Simulation results are then presented for a cellular-based ISAC scenario considering system parameterization compliant to current 5G and, finally, a discussion on open challenges for future deployments is presented.

Index Terms—6G, bistatic sensing, hardware impairments, integrated sensing and communication (ISAC), orthogonal frequency-division multiplexing (OFDM), synchronization.

I. INTRODUCTION

To exploit the inherently distributed nature of cellular networks, enabling bistatic integrated sensing and communication (ISAC) is an essential task for sixth generation (6G) networks. In the bistatic architecture, transmitter and receiver are widely separated. Besides greater sensing diversity and being a key enabler of multistatic ISAC [1], this architecture avoids full-duplex challenges faced in the monostatic case [2].

In spite of the aforementioned advantages, bistatic ISAC introduces several challenges [3]. These include required synchronization between transmitter and receiver to avoid sensing bias and overall performance degradation. Furthermore, the limited knowledge of the transmit data at the receiver for radar processing must also be accounted for. Finally, as in the monostatic case, hardware impairments must still be considered during system design in bistatic ISAC. These include, e.g., antenna non-idealities, non-linear distortions, in-phase/quadrature (I/Q) imbalance, oscillator phase noise (PN), and further impairments in data converters.

In this article, these and further practical challenges in bistatic orthogonal frequency-division multiplexing (OFDM)-based ISAC are described, and solutions in the contexts of system design and signal processing discussed.

II. NOTATION AND LINK BUDGET

The considered bistatic ISAC system is composed of two gNodeBs (gNBs) with static and known positions as depicted in Fig. 1. It is assumed that gNB #1 acts as a transmitter

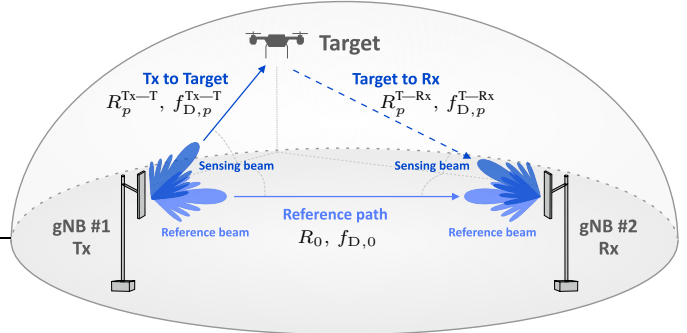


Fig. 1. Bistatic ISAC system model. In this example, a static reference path labeled as $p = 0$ and a path $p = 1$ associated with a radar target are shown.

and gNB #2 as a receiver. The OFDM signal transmitted by gNB #1 occupies a bandwidth B at a carrier frequency f_c and is derived from the discrete-frequency domain frame $\mathbf{X} \in \mathbb{C}^{N \times M}$ with $N \in \mathbb{N}_{>0}$ subcarriers and $M \in \mathbb{N}_{>0}$ OFDM symbols. Before being received by gNB #2, this signal propagates through P paths labeled as $p \in \{0, 1, \dots, P-1\}$. The path $p = 0$ is a reference path used for synchronization that also serves as a reference target for bistatic radar sensing, while the remaining $P-1$ paths are associated with radar point targets. While the reference is assumed to be a line-of-sight (LoS) path in Fig. 1, any dominant path, including non-line-of-sight (NLoS) ones, with constant range, Doppler shift, and angle could be used for the same purpose. If the reference path is a non-dominant NLoS one, the information that its parameters are constant can be used to help distinguishing it from paths associated with radar targets, therefore enabling the compensation for any eventual synchronization and target parameter estimation biases caused by a dominant radar target.

The path p is associated with delay $\tau_p = R_p/c_0$, where c_0 is the speed of light in vacuum and $R_p = R_p^{\text{Tx-T}} + R_p^{\text{T-Rx}}$ is the bistatic range, which is equal to the sum of the range $R_p^{\text{Tx-T}}$ between gNB #1 and target and the range $R_p^{\text{T-Rx}}$ between target and gNB #2. In addition, a Doppler shift $f_{D,p} = f_{D,p}^{\text{Tx-T}} + f_{D,p}^{\text{T-Rx}}$ is experienced. $f_{D,p}$ is the sum of the Doppler shifts $f_{D,p}^{\text{Tx-T}}$ and $f_{D,p}^{\text{T-Rx}}$ resulting from the relative movement of the target w.r.t. gNB #1 and gNB #2, respectively. Since the gNBs are static, it holds that $f_{D,0} = 0$ Hz. Denoting the complex baseband equivalent of the transmitted OFDM signal by gNB #1 as $x(t) \in \mathbb{C}$, the baseband receive

signal $\tilde{y}(t) \in \mathbb{C}$ at gNB #2 is ideally expressed as

$$\tilde{y}(t) = \alpha_0 x(t - \tau_0) + \sum_{p=1}^{P-1} \alpha_p x(t - \tau_p) e^{j2\pi f_{D,p} t}. \quad (1)$$

In practice, symbol time offset (STO) τ_{STO} and carrier frequency offset (CFO) f_{CFO} are experienced. In addition, several hardware impairments are experienced, and additive white Gaussian noise (AWGN) impairs the receive signal. Representing the combined effect of these impairments as the operator $\mathcal{F}_{\text{hw-imp}}\{\cdot\}$ allows writing

$$y(t) = \mathcal{F}_{\text{hw-imp}} \{ \tilde{y}(t) * \delta(t - \tau_{\text{STO}}) e^{j2\pi f_{\text{CFO}} t} \} + n(t), \quad (2)$$

where $y(t)$ is the complex baseband equivalent of the actual receive signal at gNB #2, $*$ is the convolution operator, and $n(t)$ is the AWGN. After analog-to-digital (A/D) conversion with sampling frequency f_s and period $T_s = 1/f_s$ on $y(t)$, the sequence $y[s] \in \mathbb{C}$ is produced. Due to sampling frequency offset (SFO) [4] and sampling jitter (SJ), it holds that

$$y[s] = y(t) \Big|_{t=sT_s(1-\delta_{\text{SFO}})+\tau_{\text{SJ}}[s]}. \quad (3)$$

After further processing on $y[s]$, a radar processing gain G_p is experienced, and the range-Doppler shift periodogram $\mathbf{P} \in \mathbb{C}^{N \times M}$ produced. The latter can be expressed as

$$\mathbf{P} = \tilde{\mathbf{P}} + (\mathbf{N}_{\text{AWGN}} + \mathbf{P}_{\text{art}} + \mathbf{P}_{\text{interf}}). \quad (4)$$

In this equation, $\tilde{\mathbf{P}} \in \mathbb{C}^{N \times M}$ is the periodogram that is obtained under ideal synchronization and in the absence of hardware impairments. \mathbf{N}_{AWGN} represents the AWGN $n(t)$. The matrix $\mathbf{P}_{\text{art}} \in \mathbb{C}^{N \times M}$ contains the artifacts raised, e.g., by common phase error (CPE) resulting from hardware impairments such as PN [5] or SJ [6]. Finally, the matrix $\mathbf{P}_{\text{interf}} \in \mathbb{C}^{N \times M}$ contains noise-like interference introduced by effects such as amplitude distortions or intercarrier interference (ICI) resulting from hardware impairments such as amplifier nonlinear distortion and I/Q imbalance.

For the p th target in the periodogram \mathbf{P} , a link budget analysis leads to the maximum bistatic range parameter

$$\rho_p^{\max} = \sqrt{(R_p^{\text{Tx-T}} R_p^{\text{T-Rx}})^{\max}} = \sqrt[4]{\frac{P_{\text{Tx}} G_{\text{Tx}} G_{\text{Rx}} \sigma_p \lambda^2 G_p}{(4\pi)^3 (k_B B T_t \text{NF} + I_{\text{hw-imp}}) \text{SINR}_{\text{per}}^{\min}}}. \quad (5)$$

In this equation, P_{Tx} is the transmit power, G_{Tx} and G_{Rx} are the transmit and receive antenna plus array gains, σ_p is the radar cross section (RCS) of the p th target, and $\lambda = c_0/f_c$ is the wavelength. Furthermore, $k_B B T_t \text{NF}$ is the AWGN power, in which k_B is the Boltzmann constant, T_t is the standard room temperature in Kelvin, and NF is the receiver noise figure. $I_{\text{hw-imp}}$ represents the combined power of all noise-like interference terms originating from hardware impairments, including quantization noise. Finally, $\text{SINR}_{\text{per}}^{\min}$ is the minimum required signal-to-interference-plus-noise ratio (SINR) to detect target in the periodogram and perform unbiased parameters estimation, which is around 17 dB [2].

TABLE I
CONSIDERED SYSTEM PARAMETERS

Carrier frequency (f_c)	27.4 GHz
Frequency bandwidth (B)	190 MHz
Subcarrier spacing (Δf)	120 kHz
Number of subcarriers (N)	1584
Cyclic prefix length (N_{CP})	112
OFDM symbols per frame (M)	1120
Transmit power (P_{Tx})	36 dBm
Tx/Rx antenna + array gain ($G_{\text{Tx}}, G_{\text{Rx}}$)	33 dB
Noise figure (NF)	8 dB
Number of ADC bits (N_b)	12
Modulation alphabet (\mathcal{M})	QPSK

TABLE II
SENSING KPIs FOR FULL-FRAME RADAR SIGNAL PROCESSING

Range resolution (ΔR)	$c_0/B = 1.58$ m
Max. ua. range ($R_{\max, \text{ua}}$)	$N \Delta R = 2.50$ km
Max. ISI-free range ($R_{\max, \text{ISI}}$)	$N_{\text{CP}} \Delta R = 176.65$ m
Doppler resolution (Δf_D)	$B / [(N + N_{\text{CP}}) M] = 100.07$ Hz
Max. ua. Doppler ($f_{\text{D,max,ua}}$)	$\pm M \Delta f_D / 2 = \pm 56.04$ kHz
Max. ICI-free Doppler ($f_{\text{D,max,ICI}}$)	$\pm \Delta f / 10 = \pm 12.00$ kHz
Radar processing gain (G_p)	$N M = 62.49$ dB

III. SYSTEM DESIGN

For unbiased target parameter estimation from the periodogram \mathbf{P} , synchronization between gNBs #1 and #2 is required as later described in Section IV-A. Additionally, system design must address the influence of OFDM signal parameters on sensing key performance indicators (KPIs) and the effects of hardware impairments, as detailed in the following.

A. Bistatic sensing KPIs

The influence of OFDM signal parameters on the maximum unambiguous values and resolutions for range and Doppler shift, the maximum intersymbol interference (ISI)-free range, the maximum ICI-free Doppler shift, and the radar processing gain and target SINR in the periodogram is discussed in [7]. Considering the Frequency Range 2 (FR2) OFDM parameterization based on numerology $\mu = 3$ from the 3rd Generation Partnership Project (3GPP) technical specification (TS) 38.211 for Fifth Generation New Radio (5G NR) [8], the system parameters listed in Table I are adopted. For the full-frame radar signal processing later explained in Section IV-B, the resulting bistatic sensing KPIs listed in Table II are obtained.

B. Effects of hardware impairments

To define the maximum detectable range product ρ_p^{\max} for a target with a given RCS as described by (5), estimates of expected artifact and interference levels caused by hardware impairments and observed in the form of \mathbf{P}_{imp} and $\mathbf{P}_{\text{interf}}$ are needed. The following items describes commonly experienced

hardware impairments. It is worth highlighting that these are also relevant in monostatic architectures.

1) *Antenna/array non-idealities*: Antenna/array non-idealities include, e.g., antenna element coupling and beam squint. The first results in distortion of the ideal array patterns in both transmitting and receiving arrays, besides more severe spectral regrowth when combined with power amplifier (PA) nonlinearities at the transmitter. To reduce mutual coupling between antenna elements, countermeasures must be applied during array design. As for beam squint, it happens due to slightly different delays being experienced at the different baseband (BB) and radio-frequency (RF) chains leading to the individual antennas. Its consequences are beamforming gain reduction, angular estimation bias, and inter-beam interference. Besides hardware-based countermeasures, signal processing approaches such as phase correction are possible.

2) *Amplifier non-linear distortion*: This impairment is particularly relevant in PAs when their input signal covers a wide bandwidth and has high peak-to-average power ratio (PAPR), e.g., as in the case of OFDM in 5G NR. If insufficient input back-off (IBO) relative to the input-referred 1-dB compression point (IP1dB) is not ensured, nonlinear amplitude-to-amplitude modulation (AM-AM) and amplitude-to-phase modulation (AM-PM) of the amplified signal are experienced. Consequently, in-band interference is experienced, besides spectral regrowth and resulting out-of-band (OOB) emissions specifically in the case of PAs at the transmitter.

3) *Mixer non-idealities*: Besides similar non-linear distortion as in amplifiers, frequency-selective I/Q imbalance can be experienced in quadrature mixers. This happens due to differences between the resulting channel impulse responses (CIRs) of I and Q branches due to transfer functions of analog low-pass (LP) filters as well as digital-to-analog converters (DACs) at the transmitter or analog-to-digital converters (ADCs) at the receiver. Although I/Q imbalance suppression measures can be taken during mixer design, further measures are required due to the high sensitivity of radar sensing. In [9], a blind I/Q imbalance estimation and correction approach for OFDM-based radar systems is introduced, which can be directly applied to the considered bistatic OFDM-based ISAC system.

4) *Oscillator phase noise*: PN consists of phase variations experienced due to non-idealities in the local oscillator (LO) signal that is input to the mixers at both transmitter and receiver. In OFDM-based systems, it results in CPE and ICI. The first impairs the discrete Fourier transform (DFT)-based Doppler shift estimation, leading to artifacts in the periodogram, target peak power loss, and estimation bias. As for ICI, it results in loss of orthogonality between the subcarriers. Due to the random nature of transmit data, ICI does not result in artifacts, but still leads to target peak power loss and increased interference level. To compensate these effects, PN must be estimated at least in part. A feasible countermeasure consists of estimating and compensating the CPE only [5], and leaving the PN-induced ICI to be naturally suppressed by the radar processing gain G_p . In bistatic sensing, this can be done by estimating the phase of static

reference paths [10]. Nevertheless, it must be considered that PN has a time-, and therefore range-dependent behavior, which results in increased CPE estimation error for targets associated with farther ranges than the reference path [5]. In multiple-input multiple-output (MIMO) architectures, different phase offsets may be experienced in different receive chains. This is because different delays are experienced due to hardware tolerances leading to different LO phases [11], besides slightly uncorrelated PN realizations. Consequently, different CPE is experienced at different receive chains, and direction-of-arrival (DoA) estimation may be impaired.

5) *DAC/ADC quantization*: Quantization noise results from the finite resolution of data converters. Focusing on ADCs, as its associated quantization noise is more relevant for sensing link budget, the experienced signal-to-quantization-noise ratio (SQNR) under perfect automatic gain control for a number $N_b \in \mathbb{N}_{>0}$ of ADC bits and oversampling equal to f_s/B is

$$\text{SQNR (dB)} = 6.02 N_b + 1.76 + 10 \log_{10}(f_s/B). \quad (6)$$

Due to the randomness of transmit data in OFDM signals, the radar processing gain G_p is also effective against quantization noise. Consequently, a factor $10 \log_{10}(G_p)$ is added to (6) to define the SQNR in the periodogram.

6) *DAC/ADC clipping*: The experienced clipping in DACs and ADCs happens as soon as the input or output ranges of the converter are exceeded. This effect is known as hard clipping. In amplifiers, soft clipping happens in the transition between its linear and saturation regions. Only when in full saturation, amplifiers cause hard clipping of signals. Due to the similarity of the hard clipping in DACs and ADCs and the full saturation in amplifiers, similar effects are expected during A/D and digital-to-analog (D/A) conversion.

7) *DAC/ADC sampling jitter*: SJ manifests as random deviations from the ideal sampling points, and is primarily caused by PN in the oscillators from which sampling clocks feeding DACs and ADCs are derived. As discussed in [6], SJ leads to ICI and can also result in CPE if band-pass (BP) sampling is performed, as it impairs the digital up-conversion (DUC) and digital down-conversion (DDC) to and from the digital intermediate frequency (IF) frequency. Specifically at DACs, SJ may also lead to OOB radiation. Besides countermeasures such as CPE compensation, jitter cleaning circuits can be used.

IV. SIGNAL PROCESSING

After system design, synchronization offsets between gNBs #1 and #2 must be accurately estimated and compensated, and the resulting signal processed for sensing accounting for limitations, e.g., due to cellular resource allocation. These aspects are covered in Sections IV-A and IV-B. Additionally, angular estimation in MIMO setups is discussed in Section IV-C.

A. Synchronization

To avoid periodogram distortion and enable unbiased target parameter estimation, STO, CFO, and SFO have been identified as synchronization offsets to be estimated and compensated in [4], [7]. It was shown that much finer offset estimation

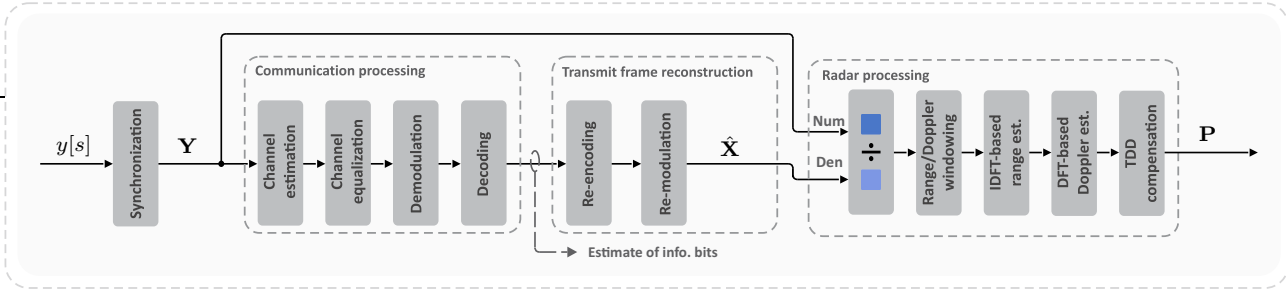


Fig. 2. Bistatic OFDM-based ISAC receiver processing chain based on full-frame approach to obtain a range-Doppler shift periodogram.

accuracy is required for bistatic sensing than for OFDM-based communication systems. The algorithm developed over the course of these studies is constituted by the following steps.

1) *Coarse time and frequency synchronization*: First, coarse STO and CFO estimates are obtained based on preambles (e.g., synchronization signal blocks in 5G NR), e.g., using cross-correlation based processing [12]. The CFO is then corrected for a reduced sample range around the coarse OFDM frame start point estimate obtained through the coarse STO estimate.

2) *Sample-level time synchronization*: A correlation of the resulting samples with one of the preamble OFDM symbols is then performed to obtain an accurate STO estimate, and therefore a sample-accurate OFDM frame start sample estimate.

3) *Sampling frequency synchronization*: Next, an OFDM frame is formed and pilot subcarriers (e.g., carrying positioning reference signal (PRS) symbols) extracted. These pilots are then used to provide consecutive delay estimates for the reference path. Based on the delay drift over time, the tilt inference of time offset (TITO) algorithm [4] is used for robust and accurate SFO estimation. Afterwards, the time-domain samples are resampled and a new OFDM frame is formed.

4) *Time and frequency synchronization fine tuning*: From the obtained frame, pilot subcarriers are again extracted and residual STO and CFO estimation is performed. At this stage, the residual delay and Doppler shift w.r.t. the reference path are estimated and corrected so that it is associated with zero range and Doppler shift. Consequently, biases in the relative range and Doppler shifts estimates for further targets are avoided.

B. Periodogram generation

After synchronization, a discrete-frequency domain receive OFDM frame $\mathbf{Y} \in \mathbb{C}^{N \times M}$ is formed, on which multiple possible radar signal processing approaches can be adopted to generate range-Doppler shift periodograms. In [7], the pilot-based and full-frame approaches are discussed. The first consists of using only known pilots for radar signal processing, which comprises symbol division, inverse discrete Fourier transforms (IDFTs) for range estimation and DFTs for Doppler shift estimation as in the monostatic case. The aforementioned known pilots can be, e.g., PRS, and the fact that only a limited set of subcarriers is used results in limited sensing performance due to lower processing gain, maximum unambiguous range and maximum unambiguous Doppler shift. As for the latter approach, it consists in obtaining a full estimate $\hat{\mathbf{X}} \in \mathbb{C}^{N \times M}$

of the transmit frame \mathbf{X} via communication signal processing, allowing the use of the whole OFDM frame for radar signal processing. Consequently, full processing gain, maximum unambiguous range and maximum unambiguous Doppler shift can be achieved, and superior sensing performance is attained. A requirement, however, is that little to no communication errors occur, which can be ensured via proper choice of modulation and coding schemes, e.g., as in [13]. Otherwise, either an increased interference level or artifacts are observed in the periodogram if modulation symbol interleaving after encoding is performed or not, respectively [7]. For both processing approaches, the radar performance parameters can be calculated as in [7].

In a cellular infrastructure-based ISAC scenario, the time-division duplexing (TDD) between periodic downlink (DL) and uplink (UL) transmissions in 3GPP-compliant communication must be considered. If the DL parts are patched together or the UL parts are blanked, both a reduction of the processing gain G_p and artifacts along the Doppler shift direction of the periodogram will be observed. In [14], a method to reconstruct the point spread function of targets based on the TDD pattern knowledge is proposed. This allows subtracting the contribution of individual point targets in the periodogram. Simulation and measurement results with a 5G NR-compliant ISAC setup with commercial communication hardware in FR2 were presented, showing that the proposed method allows distinguishing between true targets and artifacts and cleaning the periodogram to enable detecting weaker targets.

To encapsulate the concepts detailed in Sections IV-A and IV-B, Fig. 2 depicts the synchronization strategy and the periodogram generation procedure relying on full-frame processing. It is worth highlighting that the estimate of information bits shown in this figure can also be used for interference cancellation, e.g., to improve monostatic sensing or bistatic sensing involving another transmitting gNB. More specifically, these bits can be used, alongside synchronization offset and channel estimates, to reconstruct the received discrete-time domain signal, which is then subtracted from the overall signal at the receiving gNB of the bistatic pair, as described in [15].

C. Angular domain sampling and reconstruction

To perform angular estimation under the constraint of beam-formed transmission, one range-Doppler shift periodogram must be estimated per direction-of-departure (DoD)-DoA pair.

Minimal angular sampling, i.e., choice of a reduced set of DoD-DoA pairs, is especially necessary in setups with confined angular acquisition capabilities, such as those with hybrid or analog beamforming structures. As discussed in [16], the changes of angular direction between consecutive pairs demonstrate that beamforming relies on distinct orthonormal bases for transmitter and receiver, which allows the task to be divided into two one-dimensional sampling problems for the azimuth-only case. For a single uniform linear array, the Fourier duality of the unitary antenna element domain and the normalized angular frequency domains align with DFT beamforming for $\lambda/2$ spacing. As such, DFT-based sampling and interpolation schemes can be applied on a per array basis to reconstruct the angular domain. With the reconstruction of a DoD-DoA region of interest, a four-dimensional periodogram (range, Doppler shift, DoD, and DoA) is obtained.

D. Multi-target information fusion and tracking

After range, angle and Doppler shift are estimated as discussed in Sections IV-B and IV-C, they must be combined or fused. This can be achieved via tracking, which establishes a target state estimate over time, while mitigating false alarms and missed detections resulting, e.g., from clutter. In [17], an unlabeled probability hypothesis filter was applied to measured data in the range-Doppler shift domain. Sensing of up to six challenging target trajectories emulated with the R&S®AREG800A radar echo generator from Rohde & Schwarz was performed with the same ISAC setup mentioned in Section IV-B. The adopted tracking approach was able to cover target birth and death and measurement-to-target association while considering resolution limitations, and a mean absolute ranging error smaller than 1.5 m was observed.

In outdoor deployments, only approximate placement and orientation of gNBs are known, e.g., due to survey errors and mounting tolerances. Since these parameters are needed to fuse range and angle into position estimates during tracking, inaccuracies eventually lead to target parameter estimation biases. While calibration based on reference targets is a potential solution, further investigation is still needed.

V. SIMULATION RESULTS

To evaluate the effect of the discussed impairments on the sensing link budget for a bistatic OFDM-based ISAC system with the parameters from Table I, PA non-linear distortion, PN, ADC quantization, and SJ were considered and simulated. The remaining impairments were either assumed to be avoided during system design or to be compensated via signal processing, which is feasible with the discussed approaches. For the PA, a memoryless nonlinearity model based on a lookup table was used, and a 10 dB IBO from the IP1dB was considered. Regarding PN, two independent realizations of the 3GPP model for gNBs at 30 GHz proposed in [18] were simulated for transmitter and receiver, respectively, as described in [5], yielding an integrated PN level of -32.09 dBc. Due to the described reasons in Section III-B4, CPE was not compensated. Furthermore, $N_b = 12$ ADC bits as in Table I,

TABLE III
CONSIDERED IMPAIRMENTS AND SIMULATED CORRESPONDING SIR

Impairment	PPLR (dB)	Mean SIR (dB)	Min. SIR (dB)
PA nonlinearity	-0.09 dB	100.31 dB	N/A
PN	0 dB	92.23 dB	56.92 dB
ADC quantization	N/A	129.72 dB	N/A
DAC/ADC SJ	0 dB	139.18 dB	99.37 dB
All combined	-0.09 dB	91.60 dB	56.92 dB

besides $f_s = 4$ GHz and a digital IF of 1 GHz, which are, e.g., possible with the Zynq UltraScale+ RFSoC ZCU111, were assumed. The maximum signal level, which defines the quantization noise, was set as 20 dB higher than the average LoS path power to account for its PAPR and provide a margin. Finally, model parameters based on data from the data sheet for LMX2594 RF synthesizer, which is used in ZCU111 system-on-a-chip (SoC) platforms, were used to generate the PN power spectral density shaping the experienced SJ as in [6], while setting LMX2594's nominal SJ root mean square (RMS) level of 45 fs. Two independent realizations of the described process were used to simulate DAC and ADC SJ.

To obtain a sensing performance upperbound, DL-only transmission was considered. peak power loss ratio (PPLR) and periodogram signal-to-interference ratio (SIR) for a scenario with a LoS reference path and no targets were calculated assuming ideal synchronization. More specifically, a Chebyshev window with 100 dB sidelobe suppression was used for range and Doppler shift. Next, the PPLR w.r.t. a impairment-free scenario with otherwise equal settings was calculated, and the SIR was calculated as the ratio between the reference path peak and the region after a margin outside its main lobe. The obtained results are listed in Table III. For comparison, the procedures for calculating mean SIR and minimum SIR yield 153.19 dB and 100 dB, respectively, for the impairment-free case due to the sidelobes of the reference path. Note that ADC quantization noise is handled as a hardware impairment and its level is measured via SIR, which is, however, equivalent to SQNR as in (6). Since it has a purely additive noise effect, PPLR is not calculated for it. For PN and SJ, the minimum SIR is shown, as these impairments cause both uniform interference and artifacts. To calculate of the combined effect of hardware impairments, the conservative assumption that these impairments are all uncorrelated was made. Consequently, the overall PPLR is equal to the sum of the individual PPLRs in decibel scale, and the overall mean and minimum SIR results from the sum of the respective mean and maximum interference levels in linear scale.

Next, 21 dBm were allocated to the transmit beam associated with a LoS reference path with a range of 300 m, and the remaining 35.86 dBm to a sensing beam. Fig. 3 shows the power levels in the periodogram for the reference path and three targets, namely a drone (0.1 m^2 RCS), a pedestrian (1 m^2 RCS), and a car (100 m^2 RCS) [2], all enhanced by the processing gain G_p minus the combined PPLR of all impairments from Table III. While range and power for the

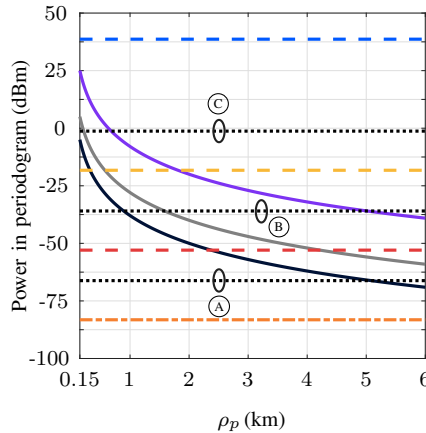


Fig. 3. Power in periodogram accounting for antenna and processing gains as a function of the range parameter $\rho_p = \sqrt{R_p^{\text{Tx-T}} R_p^{\text{T-Rx}}}$. Results are shown for a drone (—), a pedestrian (—), and a car (—). In addition, the power of the LoS path peak in the periodogram (—), its associated mean (—) and maximum (—) impairment-induced interference levels, and the AWGN (—) level are shown. Finally, the power levels (—) yielding 17 dB signal-to-noise ratio (SNR) against AWGN, 17 dB SINR against AWGN and mean interference, and 17 dB SINR against AWGN and interference-induced artifacts are marked as (A), (B), and (C), respectively.

reference path are fixed, the power levels of radar targets are shown as functions of the range parameter ρ_p of the p th target. This parameter is defined as square root of the product of the range between transmitter and target and the range between target and receiver, i.e., $\rho_p = \sqrt{R_p^{\text{Tx-T}} R_p^{\text{T-Rx}}}$. In addition, levels for AWGN, besides mean interference and artifacts due to hardware impairments, are also shown. Based on these results, the maximum ρ_p for which $\text{SINR}_{\text{per}}^{\min} \geq 17 \text{ dB}$ [2] was calculated with (5). The obtained results for ρ_p^{\max} were 0.89 km, 1.59 km, and 5.01 km for drone, pedestrian, and car, respectively, with $I_{\text{hw-imp}}$ defined by the mean interference level. In the impairment-free case, ρ_p^{\max} is equal to 5.11 km, 9.09 km, and 28.75 km, respectively, due to AWGN only and disregarding the LoS path sidelobes. If $I_{\text{hw-imp}}$ is defined by the artifact level, the ρ_p^{\max} values for drone, pedestrian, and car are reduced to 0.12 km (smaller than $\rho_0 = 150 \text{ m}$ for the reference path), 0.22 km, and 0.68 km, respectively. To avoid severe ρ_p^{\max} limitation, the mean interference level can be set as the limiting factor, and artifacts can be handled, e.g., via CPE compensation [5] or clutter removal [19].

VI. CONCLUSION

This article provided an overview of practical challenges and solutions for 6G OFDM-based bistatic ISAC. In this context, the influence of OFDM parameters on sensing KPIs and the impact of various hardware impairments were described, and key signal processing techniques discussed.

It was shown that, at first, accurate synchronization (STO, CFO, SFO) needs to be achieved between gNBs. Then, periodogram generation with either pilots or knowledge of full transmitted frame was discussed, and practical issues due to TDD patterns and angular domain sampling and reconstruction

for DoD-DoA estimation considered. In addition, considerations on challenges such as mutual interference cancellation, multi-target information fusion and tracking, and the need for robust geometry calibration, were also made. Finally, simulation results showed that hardware impairments reduce sensing performance, limiting the maximum detectable range.

ACKNOWLEDGMENTS

The authors acknowledge the financial support by the Federal Ministry of Research, Technology and Space of Germany in the project KOMSENS-6G under grant numbers 16KISK112K, 16KISK113, and 16KISK010.

REFERENCES

- [1] R. Thomä et al., "Distributed multisensor ISAC," *arXiv preprint arXiv:2511.13104 [eess.SP]*, Nov. 2025.
- [2] S. Mandelli, M. Henninger, M. Bauhofer, and T. Wild, "Survey on integrated sensing and communication performance modeling and use cases feasibility," in *2023 2nd Int. Conf. 6G Netw.*, Oct. 2023, pp. 1–8.
- [3] H. Wyneersch et al., "Cross-layer integrated sensing and communication: A joint industrial and academic perspective," *IEEE Open J. Commun. Soc. (Early Access)*, pp. 1–51, Aug. 2025.
- [4] L. Giroto de Oliveira et al., "Pilot-based SFO estimation for bistatic integrated sensing and communication," *IEEE Trans. Microw. Theory Tech.*, vol. 73, no. 7, pp. 4143–4161, Jul. 2025.
- [5] —, "On the sensing performance of OFDM-based ISAC under influence of oscillator phase noise," *arXiv preprint arXiv:2410.13336 [eess.SP]*, Oct. 2024. [Online]. Available: <https://arxiv.org/abs/2410.13336>
- [6] L. Giroto et al., "Analysis of sensing in OFDM-based ISAC under the influence of sampling jitter," *arXiv preprint arXiv:2601.14881 [eess.SP]*, Jan. 2026.
- [7] D. Brunner et al., "Bistatic OFDM-based ISAC with over-the-air synchronization: System concept and performance analysis," *IEEE Trans. Microw. Theory Tech.*, vol. 73, no. 5, pp. 3016–3029, May 2025.
- [8] 3rd Generation Partnership Project (3GPP), "Physical channels and modulation," TS 38.211, Jul. 2023, version 17.5.0.
- [9] B. Schweizer, C. Knill, D. Schindler, and C. Waldschmidt, "IQ-imbalance compensation for wideband OFDM-radar," in *2020 14th Eur. Conf. Antennas Propag.*, Mar. 2020, pp. 1–5.
- [10] D. Griffiths et al., "Phase synchronization of bistatic radar by exploiting the urban scene," *IEEE Trans. Aerosp. Electron. Syst.*, vol. 61, no. 3, pp. 6083–6097, Jun. 2025.
- [11] C. Collmann, A. Nimir, and G. Fettweis, "On the impact of phase impairments on angle estimation in true-time-delay systems," in *2025 IEEE 5th Int. Symp. Joint Commun. Sens.*, Jan. 2025, pp. 1–6.
- [12] A. Omri, M. Shaqfeh, A. Ali, and H. Alnuweiri, "Synchronization procedure in 5G NR systems," *IEEE Access*, vol. 7, pp. 41 286–41 295, Mar. 2019.
- [13] M. Henninger, L. Giroto, A. Elkelesh, and S. Mandelli, "Hybrid resource allocation scheme for bistatic ISAC with data channels," *arXiv preprint arXiv:2601.11110 [eess.SP]*, Jan. 2026.
- [14] M. Henninger, L. Giroto, S. Saur, A. Grudnitsky, T. Wild, and S. Mandelli, "Target detection for ISAC with TDD transmission," in *2025 28th Int. Workshop on Smart Antennas*, Sept. 2025, pp. 1–7.
- [15] T. Jeong et al., "Interference analysis and successive interference cancellation for multistatic OFDM-based ISAC systems," *arXiv preprint arXiv:2507.20942 [eess.SP]*, Jul. 2025.
- [16] A. Felix, S. Mandelli, M. Henninger, and S. ten Brink, "Optimal azimuth sampling and interpolation for bistatic ISAC setups," in *2025 28th Int. Workshop on Smart Antennas*, Sept. 2025, pp. 241–246.
- [17] M. Bauhofer et al., "Experimental demonstration of multi-object tracking in integrated sensing and communication," *arXiv preprint arXiv:2510.22180 [eess.SP]*, Oct. 2025.
- [18] 3rd Generation Partnership Project (3GPP), "Study on new radio access technology: Radio Frequency (RF) and co-existence aspects," TR 38.803, Mar. 2022, version 17.5.0.
- [19] M. Henninger, S. Mandelli, A. Grudnitsky, T. Wild, and S. ten Brink, "CRAP: Clutter removal with acquisitions under phase noise," in *2023 2nd Int. Conf. 6G Netw.*, Oct. 2023, pp. 1–8.